Nanoscale Advances

ROYAL SOCIETY OF CHEMISTRY

PAPER

View Article Online
View Journal | View Issue

Check for updates

Cite this: *Nanoscale Adv.*, 2023, **5**, 3084

Colorimetric mercury detection with enhanced sensitivity using magnetic-Au hybrid nanoparticles†

Miseon Jeong, Dahyun Bae and Jin-sil Choi *

Received 28th February 2023
Accepted 15th May 2023

DOI: 10.1039/d3na00129f

rsc.li/nanoscale-advances

Due to the neural toxicity of mercury, there is a need for the development of on-site detection systems for Hg^{2+} monitoring. To this end, a new colorimetric mercury detection probe, Fe_3O_4@SiO_2@Au (magnetic-Au; Mag-Au) hybrid nanoparticles, has been developed. The Au on the surface of Mag-Au is an indicator of Hg^{2+}, which forms an AuHg alloy (amalgam) on their surface (Mag-Au@Hg), with excellent peroxidase-like activity. The oxidation of 3,3′,5,5′-tetramethylbenzidine by Mag-Au@Hg resulted in a color change of the indicator solution, which was enhanced with increasing Hg^{2+} concentration. Mag-Au can be used to detect Hg^{2+} at nanomolar concentrations. Additionally, magnetic separation can be used to easily purify and concentrate the Mag-Au@Hg from samples, and thus avoid interference from unwanted residues or colored samples. The feasibility of Mag-Au for Hg^{2+} detection was tested with an artificial urine solution and it can be used to detect Hg^{2+} in various real samples, such as river water, seawater, food, and biological samples.

Open Access Article. Published on 15 May 2023. Downloaded on 12/5/2025 9:55:14 AM.
This article is licensed under a Creative Commons Attribution-NonCommercial 3.0 Unported Licence.

Introduction

The pollution caused by heavy metal ions has caused critical risks to human health and the environment worldwide.[1–5] Mercury is one of the most toxic elements; it is readily bioaccumulated and thus concentrates in raw food materials. The accumulation of trace organic mercury in the human body has a strong neurotoxic impact and can cause severe damage to the organs. In addition, mercury can participate in the methylation and demethylation processes in the gut microbiome, which influences their metabolism thereby disturbing the neural system.[6,7] Owing to the acute toxicity of mercury, the World Health Organization (WHO) and the U.S. Environmental Protection Agency have set the threshold concentration of mercury in drinking water at 2 μg L^{-1} (10 nM).[8] Traditional methods for mercury detection mainly rely on atomic absorption spectrometry, atomic fluorescence spectrometry, inductively coupled plasma optical emission spectroscopy/mass spectrometry, and electrochemical methods.[1,6] Because these methods require technically skilled operators, and are time-consuming and complex processes, it is highly desirable to develop inexpensive and facile on-site methods for mercury detection. To this end, optical analyses are promising techniques that can provide qualitative and quantitative results by naked-eye discrimination without requiring any expensive equipment.[9–20]

Recently, colorimetric sensors, where nanozymes are adopted as color converters responding to targets, have attracted interest.[1] The term 'nanozymes' refers to nanomaterials with intrinsic enzyme-like activity (*e.g.*, peroxidase, oxidase, catalase, superoxide dismutase, and hydrolase), which can efficiently catalyze substrate conversions. Compared with natural enzymes, nanozymes are advantageous in terms of cost, large-scale production, robustness to harsh environments, stability, and long-term storage. In addition, their catalytic activity can be tuned by controlling size, structure, or morphology, by introducing dopants, and by modifying surface functional groups.[21–25] Thus, several researchers have developed nanozyme-based mercury detection systems. For example, Au interacts strongly with Hg^{2+} ions forming an HgAu alloy (amalgam), which leads to a remarkable enhancement of the peroxidase-like activity of Au nanoparticles (Au NPs).[26–32] The strong chelating interaction of Hg^{2+} with Ag_2S@graphene oxide also provides an excellent synergistic catalytic effect.[33] Mercuric cations downregulate the enzymatic activities of Pt, Se, SnTe, CuS, and Co_3O_4 nanoparticles.[12,34–37] The formation of HgI reduces the peroxidase-like activity of I_2, indicating the presence of Hg *via* the color change of the solution.[38] Mercuric cations block the active sites of S-containing carbon dots and chitosan-functionalized $MoSe_2$ nanosheets, reducing their catalytic activities.[27,39] DNAzyme, rich in thymidine, is another suitable candidate for colorimetric mercury detection probes.[8,40,41] However, these colorimetric sensors are limited by the color of the samples or are needed in the pretreatment

Department of Chemical and Biological Engineering, Hanbat National University, Daejeon 34158, Korea. E-mail: jisil.choi@hanbat.ac.kr

† Electronic supplementary information (ESI) available: Synthetic protocols and TEM images of Fe_3O_4, Fe_3O_4@SiO_2, Au seeds, and Mag-Au, confirmation of amalgam formation on Mag-Au using XPS analysis, detection capability of Fe_3O_4, Fe_3O_4@SiO_2, Mag-Au, ROS generation test by Mag-Au@Hg, and comparison of catalytic effect of Mag-Au in various condition. See DOI: https://doi.org/10.1039/d3na00129f

© 2023 The Author(s). Published by the Royal Society of Chemistry

Open Access Article. Published on 15 May 2023. Downloaded on 12/5/2025 9:55:14 AM.
This article is licensed under a Creative Commons Attribution-NonCommercial 3.0 Unported Licence.

process. Herein, we have developed a Fe_3O_4@SiO_2@Au (magnetic Au; Mag-Au) hybrid nanoparticle system for mercury detection with enhanced sensitivity (Scheme 1). The Au shell of the Mag-Au system is an indicator that reacts with Hg^{2+} to form an amalgam (Mag-Au@Hg), which in turn, exhibits an enhanced peroxidase-like activity. The Mag-Au@Hg was purified and concentrated from the samples through magnetic separation. Therefore, it is possible to avoid the disturbance of enzymatic reactions by residues present in the samples and achieve clear color recognition. As a result, Hg^{2+} ions in artificial urine could be successfully monitored using the as-prepared Mag-Au hybrid nanoparticles.

Experimental section

Reagents

The following reagents and chemicals were used as received without further purification: $FeCl_3 \cdot 6H_2O$ (Sigma-Aldrich), anhydrous citric acid (99.5%, Samchun), sodium citrate dihydrate (99.0%, Daejung), anhydrous sodium acetate (NaOAc, Duksan), polyacrylic acid (PAA, MW: 5000, 50% aqueous solution, Acros Organics), tetraethyl orthosilicate (TEOS, TCI), ammonia solution (28–30%, Samchun), (3-aminopropyl)trimethoxysilane (APTMS, Sigma-Aldrich), and hydrogen tetrachloroaurate(III) hydrate (99.9% metal basis, Au 49% min Alfa Aesar), sodium hydroxide (Duksan), tetrakis(hydroxymethyl) phosphonium chloride (TCI), bis(*p*-sulfonatophenyl)phenylphosphine dihydrate dipotassium salt (BSPP, Sigma-Aldrich), anhydrous potassium carbonate (99%, Alfa Aesar), hydroxylamine hydrochloride, mercury(II) chloride (99.5%, Acros Organics), hydrogen peroxide (34.5%, Samchun), 3,3′,5,5′-tetramethylbenzidine (TMB, TCI), glacial acetic acid (Duksan), silver nitrate (99.8%, Samchun), anhydrous iron(III) chloride (98.0%, Samchun), nickel(II) chloride hexahydrate (97.0%, Samchun), cobalt(II) chloride hexahydrate (97.0%, Samchun), zinc chloride (98.0%, Samchun), copper(II) chloride dihydrate (97.0%, Daejung), manganese(II) chloride tetrahydrate (98.0%, Daejung), calcium chloride (95.0%, Duksan), sodium chloride (99.0%, Duksan), 1,3-diphenylisobenzofuran (DPBF, 97%, Alfa Aesar) and artificial urine (Pickering Laboratories, Inc.).

Equipment

The size and shape of the Mag-Au nanoparticles were analyzed *via* field emission scanning electron microscopy (Cold Type FE-SEM, S-4800, Hitachi High Technology, Japan) and transmission electron microscopy (TEM, Tecnai G2 F30 S-Twin, Netherlands). The hydrodynamic size and surface charge of Mag-Au were measured using a Zetasizer (ZSU3200, Malvern Panalytical, England). The optical and magnetic properties of Mag-Au were analyzed using a UV-VIS/NIR spectrophotometer (Lambda 1050, PerkinElmer, USA) and vibrating sample magnetometry (VMS, 7400-S, Lake Shore Cryotronics, USA), respectively. X-ray diffraction (XRD; SmartLab, Rigaku, Japan) was used to determine the crystal structure of Mag-Au. Analyses of the chemical composition of Mag-Au were performed using energy dispersive X-ray spectroscopy (EDX equipped on TEM). The absorbance of Hg^{2+} detection solution was measured using plate reader (Multi-mode microplate reader, SpectraMax M2e, Molecular devices).

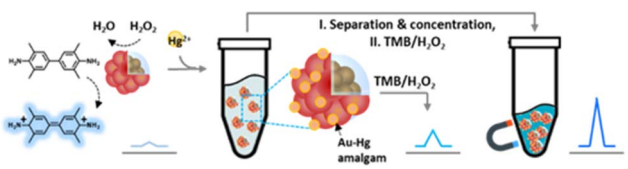

Scheme 1 Detection of Hg(II) using Mag-Au hybrid nanomaterials.

Preparation of Mag-Au NPs (Fe_3O_4@SiO_2@Au)

Fe_3O_4 nanoclusters were prepared *via* a solvothermal method[42,43] and their surfaces were further modified with SiO_2.[44] The detailed preparation protocol is described in the ESI.† The aminated Fe_3O_4@SiO_2 nanoparticles (10 mg) were incubated overnight with a concentrated Au seed solution. The unattached free Au seeds were then removed by magnetic separation. The purified Fe_3O_4@SiO_2@Au seed was mixed with the growth solution (0.2 mM, 1.6 L), 20 mL of BSPP (22.6 μM), and 32 mL of $NH_3OH \cdot HCl$ (363.2 μM) with vigorous stirring. The mixture was allowed to react for 3 days. After the reaction, the reaction solution was centrifuged and unreacted reagents in the supernatant were removed. The purified Mag-Au NPs were redispersed in DIW and were stored in the refrigerator at 4 °C before usage.

Peroxidase-like activity of Mag-Au with the existence of Hg^{2+} ions

Mag-Au (300 ng) was added to a buffer solution (citrate buffer, pH 5.4, 10 mM) containing mercury ions (10–400 nM). Subsequently, H_2O_2 (150 mM) and TMB (0.59 mM) were added rapidly. After 10 minutes, the absorbance of the resulting solution was measured at 652 nm. Mag-Au@Hg can be further purified and concentrated using a NdFeB magnet to enhance their sensitivity.

Hg^{2+} ion detection selectivity of Mag-Au

Experiments with different metals were performed to confirm the selective mercury detection of Mag-Au NPs. Mag-Au (300 ng) was added to a buffer (citrate buffer, pH 5.4, 10 mM) containing 200 nM of metal (Hg^{2+}, Ag^{+}, Fe^{3+}, Ni^{2+}, Co^{2+}, Zn^{2+}, Cu^{2+}, Mn^{2+}, Ca^{2+}, Na^{+}). H_2O_2 (130 mM, 20 μL) and TMB (0.59 mM, 20 μL) were then added rapidly. The absorbance of the resulting solution was measured at 652 nm.

Detection of Hg^{2+} in artificial urine

The artificial urine sample of Hg addict patient was prepared by adding $HgCl_2$ (1.1 μM, 10 μL) to artificial urine. Mag-Au (30 μg mL^{-1}) were added to artificial urine, first. Then the mixture were mixed with pH 5.4 buffer (citrate buffer, 10 mM), H_2O_2 (150 mM), and TMB (0.59 mM). After 10 minutes of mixing, the

© 2023 The Author(s). Published by the Royal Society of Chemistry

Open Access Article. Published on 15 May 2023. Downloaded on 12/5/2025 9:55:14 AM.
This article is licensed under a Creative Commons Attribution-NonCommercial 3.0 Unported Licence.

absorbance of the solution was measured at 652 nm using a multimode plate reader.

Results and discussion

The Mag-Au nanoparticles were obtained by the sequential synthesis of the iron oxide core, intermediate SiO_2 layer, and Au shell (Fig. 1a). The Au shell was easily grown from Au seeds with a surface charge of −30.4 mV, which were bound to the aminated silica shell on Fe_3O_4 with a surface charge of +46.49 mV *via* electrostatic interactions (Fig. S1 and S2†). As shown in the SEM and TEM images (Fig. 1b–d and S2†), the size of the nanoparticles gradually increases after the surface coating with silica and sequential growth of the Au shell without additional seed formation. The size of the Fe_3O_4 nanoclusters is 151.8 ± 29.7 nm, and that of Mag-Au increases to 233.7 ± 59.0 nm. The hydrodynamic size of Mag-Au is 491.5 nm, which is larger than the size observed in the SEM images. As shown in the high-resolution TEM image, crystalline Au particles of a few nanometers in size were grown on the amorphous SiO_2 layer, forming an Au shell (Fig. S3†). The EDX mapping of the Mag-Au nanoparticles shows the distribution of Fe (yellow), Si (red),

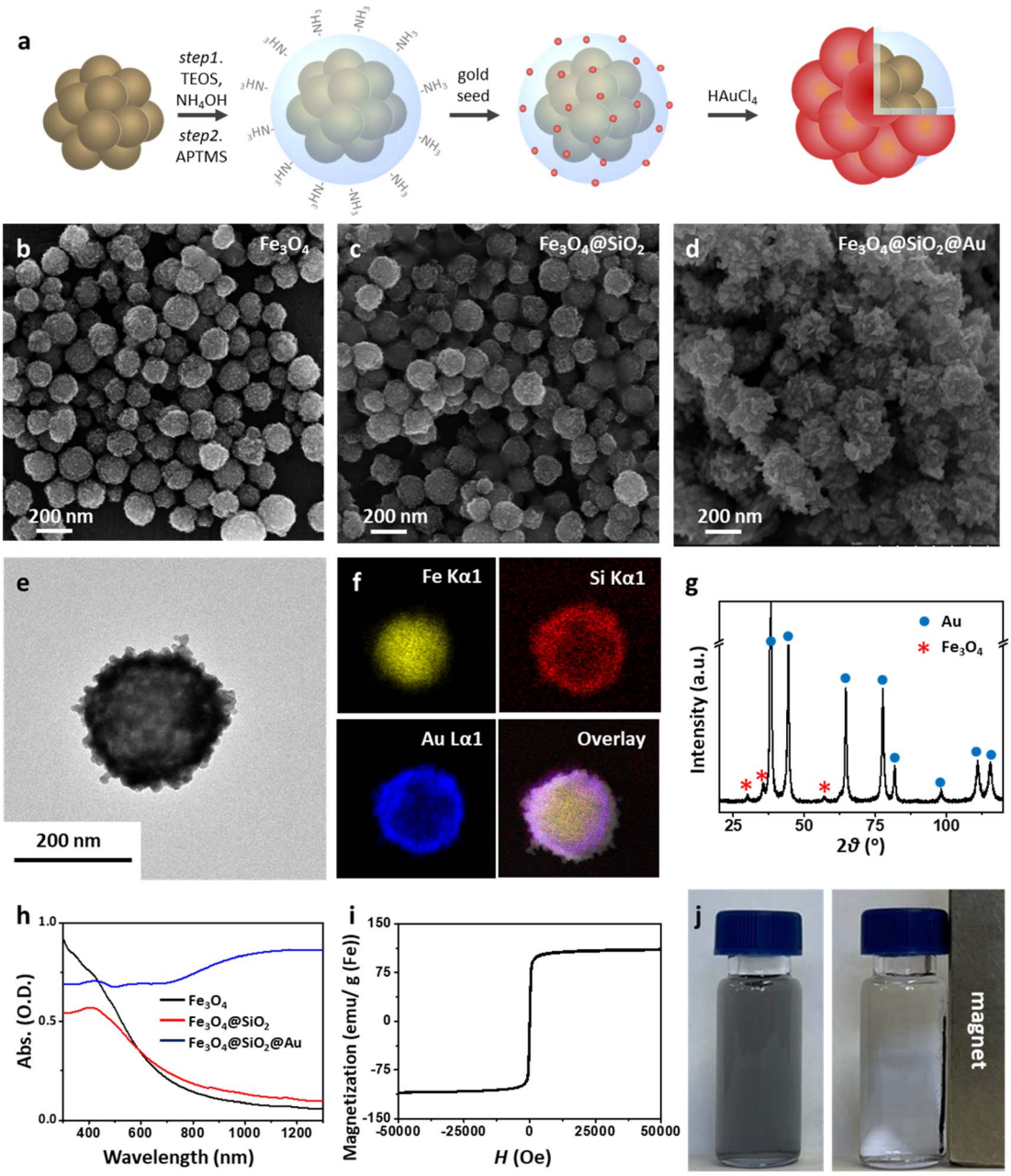

Fig. 1 (a) Schematic of Mag-Au synthesis. SEM images of (b) Fe_3O_4, (c) Fe_3O_4@SiO_2, and (d) Fe_3O_4@SiO_2@Au (Mag-Au). (e and f) TEM and color-mapped STEM images of Mag-Au to observe the distribution of elements. (g) XRD, (h) optical, and (i) magnetic analyses of Mag-Au. (j) Images of the solutions containing Mag-Au, wherein a NdFeB magnet is placed beside the vial.

© 2023 The Author(s). Published by the Royal Society of Chemistry

Open Access Article. Published on 15 May 2023. Downloaded on 12/5/2025 9:55:14 AM.
This article is licensed under a Creative Commons Attribution-NonCommercial 3.0 Unported Licence.

and Au (blue), and the core–shell structure was clearly visualized (Fig. 1f). According to EDX analysis, the as-prepared Mag-Au comprises 31.3% (Fe), 11.6% (Si), and 57.1% (Au) (Table S1†). The XRD spectrum exhibits peaks from both the Au shell and Fe_3O_4 core (Fig. 1g). The Mag-Au hybrid nanoparticles show strong absorption in the NIR region (>700 nm) as compared to Fe_3O_4 and Fe_3O_4@SiO_2 nanoparticles (Fig. 1h); this can be attributed to the Au shell in the hybrid clusters. In addition, the Mag-Au nanoparticles are superparamagnetic with a high value of saturation magnetization, comparable with that of similar-sized Fe_3O_4 nanoparticles (Fig. 1i).[43] Therefore, Mag-Au nanoparticles can strongly influence the response to the magnet, although they are well-dispersed in an aqueous solution without the magnet (Fig. 1j).

The enzymatic activity of Au nanoparticles is enhanced by the formation of an amalgam with Hg^{2+}; thus, several studies explore the use of Au hybrid nanoparticles for Hg^{2+} detection.[26,28,30,45] To examine the possibility of using Mag-Au hybrid nanoparticles for Hg^{2+} ion detection, the peroxidase-like activity of the Mag-Au hybrid nanoparticles was compared in the presence and absence of Hg^{2+} (Fig. 2a). When a TMB (0.59 mM)/H_2O_2 (150 mM) solution was mixed with the Mag-Au hybrid nanoparticles, the color of the solution changed slightly to a light blue color (Fig. 2b) due to its peroxidase-like activity.[46] In contrast, the color of the solution turned blue when Hg^{2+} ions (200 nM) were premixed with the Mag-Au hybrid nanoparticles (Fig. 2b). When the time-dependent absorbance variation at 652 nm was monitored, the absorbance of the solution containing Hg(II) premixed with Mag-Au hybrid nanoparticles dramatically increased compared to that of the solution with pristine Mag-Au hybrid nanoparticles (Fig. 2c). Considering no absorbance change was absorbed with Fe_3O_4 and Fe_3O_4@SiO_2 under same experiment (Fig. S4†), formation of amalgam on Au shell on Mag-Au is key reaction to detect Hg^{2+}. The color mapped EDX images of Mag-Au after the reaction with Hg^{2+} ions show Hg distribution at the similar position of Au shell (Fig. S5†). In the XPS spectrum of Mag-Au that was purified after the reaction with Hg^{2+} ions, new peaks from Hg $4f_{5/2}$ and Hg $4f_{7/2}$ appeared (Fig. S6†). In the high resolution XPS spectrum, Hg oxidation state is determined mostly as zero based on the reported XPS values[47,48] on Mag-Au after the reaction with Hg^{2+} ions, indicating the formation of a HgAu amalgam on the Au shell.[45] The citrate, buffer in our system, can help the reduction of Hg(II) ions to Hg(0) (Fig. S7†).[26,49,50] After the reaction with TMB and H_2O_2, the oxidation state of most Hg in Mag-Au@Hg turned to 2+ (Fig. S6d and e†). Hg, which possesses smaller electronegativity compared to Au, can transfer electrons to nearby molecules through its oxidation.[26]

Based on the reactive oxygen species (ROS) indication test using 1,3-diphenylisobenzofuran, Mag-Au@Hg is capable of generating ROS and decomposing H_2O_2 more efficiently than Mag-Au (Fig. S8†). Among a range of metal ions studied, the Mag-Au hybrid nanoparticles show an enhanced enzymatic activity only in the presence of Hg^{2+} (Fig. 3). Therefore, the Mag-Au hybrid nanoparticles can be successfully used as highly selective Hg^{2+} detection probes.

The optimum reaction conditions for Hg^{2+} ion detection were explored. The peroxidase-like activity of the Mag-Au@Hg is maximum at a pH of 5.4 (Fig. S9†). The catalytic effect of Mag-Au accelerates with increasing H_2O_2 concentration, and plateaus at 150 mM H_2O_2 (Fig. S10†). Subsequently, the concentration range of Hg^{2+} that can be detected by Mag-Au was examined. The detection efficiency of Mag-Au peaks at a Hg^{2+} concentration of 30 μg mL^{-1} and then decreases at higher concentrations due to the formation of 3,3′,5,5′-tetramethylbenzidine diimine through a two-electron oxidation of TMB,[51] which shows a weak absorption at 652 nm (Fig. S11†). The indicator solution containing TMB and H_2O_2, undergoes a color change after the reaction of Mag-Au with Hg^{2+} ions (0–400 nM). With the naked eye, a weak blue color is observed in the indicator solution mixed with 50 nM Hg^{2+} ions, and a clear blue color is noted at Hg^{2+} concentrations > 100 nM (Fig. 4a). The absorption intensity at 652 nm plotted against the Hg^{2+} ion concentration depicts a gradual increase in the absorption intensity from 50 to 200 nM Hg^{2+} (Fig. 4b). Below a concentration of 100 nM Hg^{2+}, the difference in absorption intensity of the indicator solution with and without Hg^{2+} ions is not significant, which is similar to the observation with the naked eye (Fig. 4a). However, it increases considerably when the concentration of Hg^{2+} ions is >100 nM. However, the color change of the indicator solution is not clear enough to be recognized *via* a visual inspection at low concentrations.

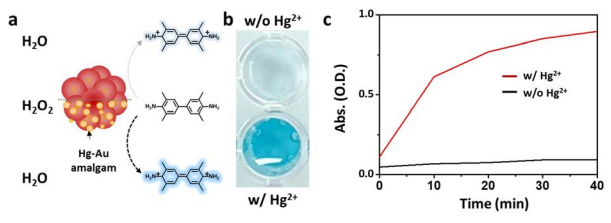

Fig. 2 (a) Schematic of the peroxidase-like catalytic reaction of Mag-Au with and without Hg^{2+}. Comparison of TMB oxidation by Mag-Au with and without Hg^{2+} through color change (b) and absorption intensity variation (c) of a mixture containing Mag-Au, TMB, and H_2O_2.

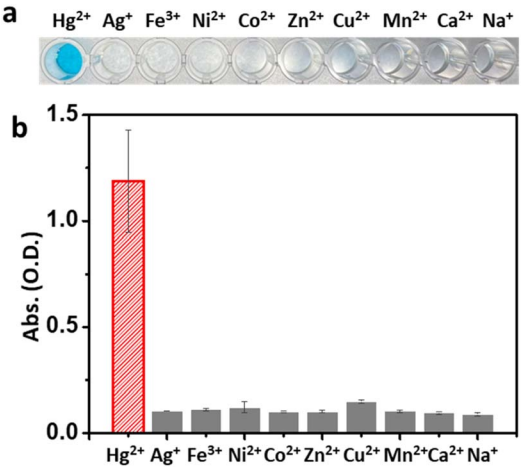

Fig. 3 Selective mercury(II) detection of Mag-Au. Comparison of TMB oxidation by Mag-Au with various metal ions through color change (a) and absorption intensity variation (b) of mixture solution containing Mag-Au, TMB, and H_2O_2.

Open Access Article. Published on 15 May 2023. Downloaded on 12/5/2025 9:55:14 AM.
This article is licensed under a Creative Commons Attribution-NonCommercial 3.0 Unported Licence.

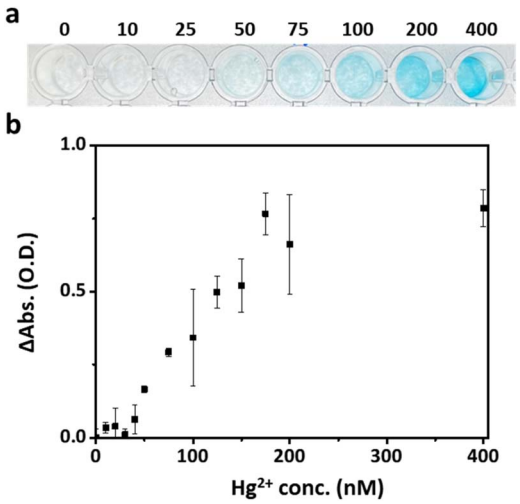

Fig. 4 Hg^{2+} concentration-dependent (a) color change and (b) absorption intensity at 652 nm of indicator solution containing Mag-Au@Hg, TMB, and H_2O_2.

To address this limitation, the Mag-Au particles were further concentrated and purified *via* magnetic separation. Magnetic separation is a convenient method for purifying and concentrating magnetically tagged substances in mixtures. Owing to the strong response of Mag-Au to external magnets (Fig. 1i and j), the Mag-Au@Hg was successfully attracted to a magnet and concentrated by removing the supernatant and redispersing it in the desired volume of citrate buffer (pH 5.4). At Mag-Au@Hg concentrations of ten times the initial concentration, the color of the indicator solution turns blue (Fig. 5a and b). As shown in Fig. 5b, the blue color of the indicator solution is clearly observed compared to that of the original solution (Fig. 4a) at various concentrations of Hg^{2+} ions. The absorption intensity (at 652 nm) of the indicator solution is highly enhanced after the magnetic concentration step (Fig. 5c). In some studies, Fe_3O_4 nanoparticles have been used for facilitating the magnetic separation to remove the unreacted probes for Hg^{2+} detection,[52,53] but not to concentrated probes in the solution. However, our study shows that the concentration of the Hg^{2+} reacted with the probe itself can influence the detection efficiency. As a result, lower concentrations of mercury can be detected with the naked eye; this method can be easily used for mercury detection in various environments.

Another advantage of the magnetic separation capability of Mag-Au is the purification of the probes from undesired residues in the samples. The amount of Hg^{2+} added is determined by measuring its concentration in urine or blood; the threshold concentration of Hg^{2+} in urine for Hg addict determination is 1.1 μM according to the WHO guidelines.[2]

Real samples contain a large number of proteins, salts, or molecules that disturb the color recognition or the reaction between Hg^{2+} ions and the probe. Therefore, Hg^{2+} detection capability of Mag-Au were examined with the similar condition of real samples. To imitate the real sample, Hg^{2+} ions (1.1 μM) were mixed in artificial urine, which possesses the same composition as urine. A droplet of the Hg-containing artificial urine (Hg^{2+} concentration in the control sample: 0 μM, Hg-addict-imitation sample: 1.1 μM) was reacted with Mag-Au, and the presence of Hg^{2+} was confirmed by the color change in the indicator solution (Fig. 6a). Without separation of Mag-Au@Hg (①), neither the control sample nor the Hg-added sample showed a recognizable color change. The formation rate of the amalgam reduces in urine, and some undesired components of urine (*e.g.*, ascorbic acid) may prohibit the oxidation of TMB.[54] Whereas, the purification and concentration of Mag-Au@Hg can improve the colorimetric signal intensity (②). As shown in Fig. 6b (inset), a clear blue color is observed in the Hg-added sample, whereas the color of the solution does not change substantially from that

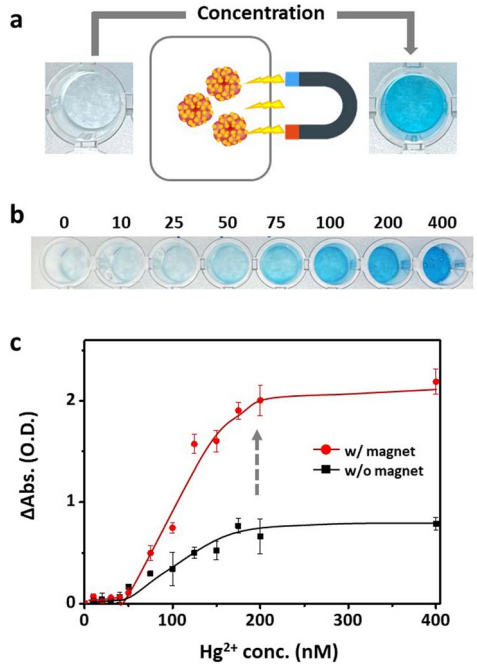

Fig. 5 (a) Comparison of the color of indicator solution before and after the concentration (10×) *via* magnetic separation. (b) Photograph of indicator solution reacted with varying concentrations of Hg^{2+} ions after the concentration *via* magnetic separation. (c) The graph of Hg^{2+} ion concentration *vs.* absorption intensity (@ 652 nm) of the indicator solution before (black, square) and after (red, circle) the concentration *via* magnetic separation.

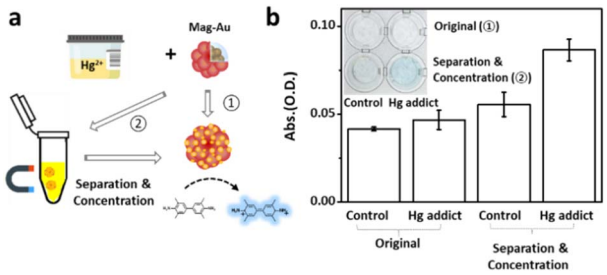

Fig. 6 (a) Schematic of the detection of Hg^{2+} ions in artificial urine. (b) Graph of absorbance of indicator solution with artificial urine in the normal condition (control) and Hg-added solution before and after the magnetic separation and concentration step. Inset: image of the four-indicator solution.

© 2023 The Author(s). Published by the Royal Society of Chemistry

Open Access Article. Published on 15 May 2023. Downloaded on 12/5/2025 9:55:14 AM. This article is licensed under a Creative Commons Attribution-NonCommercial 3.0 Unported Licence.

of the control sample. The absorbance intensity of the purified and concentrated Mag-Au@Hg in the Hg-addict-imitation sample (Fig. 6b) shows a considerably higher absorbance than those of the other samples. Thus, the magnetic separation capability of Mag-Au can greatly enhance the sensitivity of colorimetric sensors, where the existence of trace analytes can be detected with the naked eye.

Conclusions

The study developed Mag-Au hybrid nanoparticles as effective mercury probes, with the Au shell forming an HgAu amalgam that accelerates TMB oxidation. Owing to the strong response of Mag-Au to an external magnet, the Mag-Au@Hg can be purified and concentrated *via* magnetic separation so that the blue color, which originates from the oxidized TMB by Mag-Au@Hg, is clearly observed. The purification and concentration of Mag-Au@Hg can be performed using the Mag-spinner system developed by our group[43] without any complex equipment when the conditions are optimized in further studies. The improvement of color intensity through the concentration of Mag-Au@Hg can enhance the accuracy of mercury detection, thus is helpful in on-site detection systems, which are lacked of equipment. In addition, Hg^{2+} ions are readily recognized using Mag-Au by a visual inspection without interference from other residues in the sample. This separation and concentration capability of Mag-Au can allow for its application in detecting mercury in colored and blood samples. Therefore, Mag-Au can be used as an on-site Hg^{2+} detection probe for various industrial and healthcare purposes, such as water pollution monitoring, food management, work environment management, and monitoring of mercury accumulation in the living body.

Author contributions

Conceptualization, data curation, funding acquisition, investigation methodology, project administration, supervision, writing – review & editing: JC; formal analysis, validation, visualization: MJ and DB; writing – original draft: JC, MJ, and DB.

Conflicts of interest

There are no conflicts to declare.

Acknowledgements

This work was supported by National Research Foundation of Korea (NRF) grants funded by the Korean government (MSIT) (2019R1G1A109572811, 2020R1C1C101186313, 2020R1A5A801767114 and 2023R1A2C100509111).

References

1 A. Hasan, N. M. Q. Nanakali, A. Salihi, B. Rasti, M. Sharifi, F. Attar, H. Derakhshankhah, I. A. Mustafa, S. Z. Abdulqadir and M. Falahati, *Talanta*, 2020, **215**, 120939.
2 L. Magos and T. W. Clarkson, *Annals of Clinical Biochemistry: International Journal of Laboratory Medicine*, 2006, **43**, 257–268.
3 A. Alengebawy, S. T. Abdelkhalek, S. R. Qureshi and M.-Q. Wang, *Toxics*, 2021, **9**, 42.
4 J. Briffa, E. Sinagra and R. Blundell, *Heliyon*, 2020, **6**, e04691.
5 X. Li, A. D. Brejnrod, M. Ernst, M. Rykær, J. Herschend, N. M. C. Olsen, P. C. Dorrestein, C. Rensing and S. J. Sørensen, *Environ. Int.*, 2019, **126**, 454–467.
6 X. Liu, Y. Yao, Y. Ying and J. Ping, *TrAC, Trends Anal. Chem.*, 2019, **115**, 187–202.
7 F. Giambò, S. Italia, M. Teodoro, G. Briguglio, N. Furnari, R. Catanoso, C. Costa and C. Fenga, *World Academy of Sciences Journal*, 2021, **3**, 19.
8 Y. Hao, Q. Guo, H. Wu, L. Guo, L. Zhong, J. Wang, T. Lin, F. Fu and G. Chen, *Biosens. Bioelectron.*, 2014, **52**, 261–264.
9 Z. Chen, C. Zhang, Y. Tan, T. Zhou, H. Ma, C. Wan, Y. Lin and K. Li, *Microchim. Acta*, 2015, **182**, 611–616.
10 Y. Ma, L. Jiang, Y. Mei, R. Song, D. Tian and H. Huang, *Analyst*, 2013, **138**, 5338.
11 J. R. Zhang, W. T. Huang, A. L. Zeng, H. Q. Luo and N. B. Li, *Biosens. Bioelectron.*, 2015, **64**, 597–604.
12 Y. Fang, Y. Zhang, L. Cao, J. Yang, M. Hu, Z. Pang and J. He, *ACS Appl. Mater. Interfaces*, 2020, **12**, 11761–11768.
13 W. H. Danial, N. A. S. Mohamed and Z. A. Majid, *Carbon Lett.*, 2022, **32**, 57–80.
14 Y. Jiang, J. Tian, K. Hu, Y. Zhao and S. Zhao, *Microchim. Acta*, 2014, **181**, 1423–1430.
15 C. Sun, R. Sun, Y. Chen, Y. Tong, J. Zhu, H. Bai, S. Zhang, H. Zheng and H. Ye, *Sens. Actuators, B*, 2018, **255**, 775–780.
16 H. Chen, X. Zhang, H. Sun, X. Sun, Y. Shi, S. Xu and Y. Tang, *Analyst*, 2015, **140**, 7170–7174.
17 H.-H. Deng, B.-Y. Luo, S.-B. He, R.-T. Chen, Z. Lin, H.-P. Peng, X.-H. Xia and W. Chen, *Anal. Chem.*, 2019, **91**, 4039–4046.
18 Z.-X. Wang, Y.-X. Guo and S.-N. Ding, *Microchim. Acta*, 2015, **182**, 2223–2231.
19 R. S. Lankone, K. E. Challis, Y. Bi, D. Hanigan, R. B. Reed, T. Zaikova, J. E. Hutchison, P. Westerhoff, J. Ranville, H. Fairbrother and L. M. Gilbertson, *Environ. Sci.: Nano*, 2017, **4**, 1784–1797.
20 H. Singh, A. Bamrah, S. K. Bhardwaj, A. Deep, M. Khatri, R. J. C. Brown, N. Bhardwaj and K.-H. Kim, *Environ. Sci.: Nano*, 2021, **8**, 863–889.
21 D. Jiang, D. Ni, Z. T. Rosenkrans, P. Huang, X. Yan and W. Cai, *Chem. Soc. Rev.*, 2019, **48**, 3683–3704.
22 Y. Huang, J. Ren and X. Qu, *Chem. Rev.*, 2019, **119**, 4357–4412.
23 Q. Wang, H. Wei, Z. Zhang, E. Wang and S. Dong, *TrAC, Trends Anal. Chem.*, 2018, **105**, 218–224.
24 D. He, M. Yan, P. Sun, Y. Sun, L. Qu and Z. Li, *Chin. Chem. Lett.*, 2021, **32**, 2994–3006.
25 X. Wang, H. Wang and S. Zhou, *J. Phys. Chem. Lett.*, 2021, **12**, 11751–11760.
26 Z. Chen, C. Zhang, Q. Gao, G. Wang, L. Tan and Q. Liao, *Anal. Chem.*, 2015, **87**, 10963–10968.

© 2023 The Author(s). Published by the Royal Society of Chemistry

Open Access Article. Published on 15 May 2023. Downloaded on 12/5/2025 9:55:14 AM.
This article is licensed under a Creative Commons Attribution-NonCommercial 3.0 Unported Licence.

27 P. Borthakur, P. K. Boruah and M. R. Das, *ACS Sustainable Chem. Eng.*, 2021, **9**, 13245–13255.
28 R. Zhu, Y. Zhou, X.-L. Wang, L.-P. Liang, Y.-J. Long, Q.-L. Wang, H.-J. Zhang, X.-X. Huang and H.-Z. Zheng, *Talanta*, 2013, **117**, 127–132.
29 G.-H. Chen, W.-Y. Chen, Y.-C. Yen, C.-W. Wang, H.-T. Chang and C.-F. Chen, *Anal. Chem.*, 2014, **86**, 6843–6849.
30 L. Zhi, S. Zhang, M. Li, J. Tu and X. Lu, *ACS Appl. Mater. Interfaces*, 2022, **14**, 9442–9453.
31 J. Lou-Franco, B. Das, C. Elliott and C. Cao, *Nano-Micro Lett.*, 2021, **13**, 10.
32 B. Das, J. L. Franco, N. Logan, P. Balasubramanian, M. I. Kim and C. Cao, *Nano-Micro Lett.*, 2021, **13**, 193.
33 Q. Zhao, W. Gou, X. Zhang, M. Zhang, Y. Bu, L. Wang, L. Hu, W. Yao and Z. Yan, *Appl. Surf. Sci.*, 2021, **545**, 148973.
34 W. Li, B. Chen, H. Zhang, Y. Sun, J. Wang, J. Zhang and Y. Fu, *Biosens. Bioelectron.*, 2015, **66**, 251–258.
35 H. Cao, J. Xiao and H. Liu, *Biochem. Eng. J.*, 2019, **152**, 107384.
36 W. Zou, Y. Tang, H. Zeng, C. Wang and Y. Wu, *J. Hazard. Mater.*, 2021, **417**, 125994.
37 M. Zhang, Y. Qu, D. Li, X. Liu, Y. Niu and Y. Xu, *Anal. Chem.*, 2021, **93**, 10132–10140.
38 Y. Wang, L. Xu and W. Xie, *Microchem. J.*, 2019, **147**, 75–82.
39 L. Huang, Q. Zhu, J. Zhu, L. Luo, S. Pu, W. Zhang, W. Zhu, J. Sun and J. Wang, *Inorg. Chem.*, 2019, **58**, 1638–1646.
40 K. Yang, M. Zeng, X. Hu, B. Guo and J. Zhou, *Analyst*, 2014, **139**, 4445.
41 R. Tian, X. Chen, N. Jiang, N. Hao, L. Xu and C. Yao, *J. Mater. Chem. B*, 2015, **3**, 4805–4813.
42 M. Jeong, S. Lee, D. Y. Song, S. Kang, T.-H. Shin and J. Choi, *ACS Omega*, 2021, **6**, 31161–31167.
43 S. Lee, M. Jeong, S. Lee, S. H. Lee and J. Choi, *Nanoscale Adv.*, 2022, **4**, 792–800.
44 B. Luo, X.-J. Song, F. Zhang, A. Xia, W.-L. Yang, J.-H. Hu and C.-C. Wang, *Langmuir*, 2010, **26**, 1674–1679.
45 W. Qi, Y. Wang, J. Wang and C. Huang, *Sci. China: Chem.*, 2012, **55**, 1445–1450.
46 J. Li, W. Liu, X. Wu and X. Gao, *Biomaterials*, 2015, **48**, 37–44.
47 X. Guo, M. Li, A. Liu, M. Jiang, X. Niu and X. Liu, *Water*, 2020, **12**, 2105.
48 G.-W. Wu, S.-B. He, H.-P. Peng, H.-H. Deng, A.-L. Liu, X.-H. Lin, X.-H. Xia and W. Chen, *Anal. Chem.*, 2014, **86**, 10955–10960.
49 J.-Y. Yang, X.-D. Jia, X.-Y. Wang, M.-L. Chen, T. Yang and J.-H. Wang, *Analyst*, 2020, **145**, 5200–5205.
50 I. Ojea-Jiménez, X. López, J. Arbiol and V. Puntes, *ACS Nano*, 2012, **6**, 2253–2260.
51 P. D. Josephy, T. Eling and R. P. Mason, *J. Biol. Chem.*, 1982, **257**, 3669–3675.
52 L. Wang, F. Liu, N. Sui, M. Liu and W. W. Yu, *Microchim. Acta*, 2016, **183**, 2855–2860.
53 G. Wang, H. Huang, X. Zhang and L. Wang, *Biosens. Bioelectron.*, 2012, **35**, 108–114.
54 V.-D. Doan, V.-C. Nguyen, T.-L.-H. Nguyen, A.-T. Nguyen and T.-D. Nguyen, *Spectrochim. Acta, Part A*, 2022, **268**, 120709.

© 2023 The Author(s). Published by the Royal Society of Chemistry